ISSN 0036-0236, Russian Journal of Inorganic Chemistry, 2020, Vol. 65, No. 5, pp. 711–719. © Pleiades Publishing, Ltd., 2020.
Russian Text © The Author(s), 2020, published in Zhurnal Neorganicheskoi Khimii, 2020, Vol. 65, No. 5, pp. 660–668.

THERMODYNAMICS OF INORGANIC COMPOUNDS

$Pb_{0.5 + x}Mg_xZr_{2 - x}(PO_4)_3$ ($x = 0$, 0.5) Phosphates: Structure and Thermodynamic Properties

P. A. Mayorov[a], E. A. Asabina[a], V. I. Pet'kov[a], A. V. Markin[a, *], N. N. Smirnova[a], and A. M. Kovalsky[b]

[a] *National Research Lobachevsky State University of Nizhny Novgorod, Nizhny Novgorod, 603950 Russia*
[b] *National Research University of Science and Technology "Moscow Institute of Steels and Alloys", Moscow, 119049 Russia*
**e-mail: markin@calorimetry-center.ru*

Received October 22, 2019; revised November 6, 2019; accepted December 27, 2019

Abstract—Crystalline $Pb_{0.5 + x}Mg_xZr_{2 - x}(PO_4)_3$ ($x = 0$, 0.5) phosphates of $NaZr_2(PO_4)_3$ (NZP) structural type were synthesized. The heat capacity of $Pb_{0.5}Zr_2(PO_4)_3$ was measured by adiabatic vacuum and differential scanning calorimetry (DSC) within the temperature range 8–660 K. The studied phosphates were found to experience a reversible phase transition in the region 256–426 K. According to the results of Rietveld structural study, this transition occurred due to an increase in disorder of lead cation positions in cavities of the NZP structure. The measurements of $PbMg_{0.5}Zr_{1.5}(PO_4)_3$ heat capacity in the temperature range 195–660 K showed that it experienced a similar phase transition at 255–315 K. Based on the measured experimental data, the thermodynamic functions of $Pb_{0.5}Zr_2(PO_4)_3$, such as $C_p^0(T)$, $[H^0(T) - H^0(0)]$, $S^0(T)$, and $[G^0(T) - H^0(0)]$ were calculated for the temperature range 0–660 K. The standard formation enthalpy of $Pb_{0.5}Zr_2(PO_4)_3$ was determined at 298.15 K.

Keywords: phosphates, lead, NZP structural type, heat capacity, polymorphic transition, thermodynamic functions

DOI: 10.1134/S0036023620050137

INTRODUCTION

Phosphates with mixed $\{[L_2(PO_4)_3]^{p-}\}_{3\infty}$ octahedral–tetrahedral frameworks ($NaZr_2(PO_4)_3$ (NZP, NASICON, kosnarite), $Sc_2(WO_4)_3$ (SW), $K_2Mg_2(SO_4)_3$ (langbeinite), etc.) are intensively studied due to their chemical, thermal and radiation stability, and controllable (including ultrasmall) thermal expansion [1–3]. Such compounds are of interest as matrix materials for the immobilization of toxic elements, in particular, heavy metals (Pb, Cd, Sr, etc.) from industrial wastes, including radioactive ones [4, 5]. In the work [6], we have studied the possibility of incorporating the elements in the oxidation state of +2 into the structure of framework phosphates to demonstrate that the series containing large M^{2+} cations (beginning from cadmium) crystallize in the NZP structural type. In the present work, two lead-containing NZP phosphates $Pb_{0.5 + x}Mg_xZr_{2 - x}(PO_4)_3$ with $x = 0$ and 0.5 were selected as the subjects of study.

The crystallochemical formula of NZP phosphates is $(M1)_{0 \to 1}(M2)_{0 \to 3}\{[L_2(PO_4)_3]^{p-}\}_{3\infty}$, where L is the octahedrally coordinated cationic positions of framework-forming cations, and the framework itself is built of LO_6 and PO_4 polyhedra, $(M1)_{0 \to 1}$ and $(M2)_{0 \to 3}$ are the types of cationic positions in framework cavities with the number of occupied positions in each type (inside the columns of polyhedra (M1) abd between them (M2)).

Depending on the specifics of cation distribution in the cavities and the negligible displacements of framework ions, it is possible to observe a slight distortion of a cell and a change of symmetry. The highest possible symmetry of an NZP structure can be observed for the family parent $NaZr_2(PO_4)_3$, which crystallizes in space group $R\bar{3}c$ ($Z = 6$). However, the ordering of alkali-earth metal cations M^{2+} in the M1 cavities of some $M_{0.5}Zr_2(PO_4)_3$ compounds [7] leads to the splitting of each extraframework M1 position into two positions and the alternation of populated and vacant positions inside the columns. These phosphates are characterized by space group $R\bar{3}$.

Based on the literature data, it is possible to state that the framework of the $Pb_{0.5}Zr_2(PO_4)_3$ structure ($x = 0$) is built of ZrO_6 octahedra and PO_4 tetrahedra, and Pb^{2+} occupy half of the available M1 positions in the cavities. The partial substitution of zirconium by magnesium ions in the framework of the

$PbMg_{0.5}Zr_{1.5}(PO_4)_3$ structure ($x = 0.5$) leads to the complete population of M1 cavities by Pb^{2+} ions.

For the $Pb_{0.5 + x}Mg_xZr_{2 - x}(PO_4)_3$ phosphates, the synthesis and phase formation conditions were studied, and the regions of solid solutions were revealed [6]. The thermal expansion of $PbMg_{0.5}Zr_{1.5}(PO_4)_3$ within a temperature range of 293–1073 K characterizes this compound as a low-expansion material resistant to thermal shocks. However, to provide the complete characterization of the thermal behavior of lead-containing ceramics, it is necessary to have the information about their fundamental properties, such as the heat capacity, the thermodynamic functions, and the thermodynamic characteristics of phase transitions.

In the present work, the heat capacity–temperature dependence $C_p^0 = f(T)$ and crystal structure of $Pb_{0.5 + x}Mg_xZr_{2 - x}(PO_4)_3$ ($x = 0$, 0.5) NZP phosphates were studied, and their thermodynamic functions were determined in the region of 8–660 K.

EXPERIMENTAL

Phosphates $Pb_{0.5}Zr_2(PO_4)_3$ ($x = 0$) and $PbMg_{0.5}Zr_{1.5}(PO_4)_3$ ($x = 0.5$) were synthesized by the sol–gel method with subsequent heat treatment. The used initial reagents of specialty grade were $Pb(NO_3)_2$, MgO, $ZrOCl_2 \cdot 8H_2O$, and $NH_4H_2PO_4$. Before synthesis, magnesium oxide was dissolved in a calculated amount of nitric acid and the other reagents were in distilled water.

The phosphates were synthesized by pouring together aqueous solutions of metal salts in stoichiometric amounts under continuous stirring at room temperature with further addition of an ammonium dihydrophosphate solution also in compliance with the stoichiometry of these phosphates under stirring. The reaction mixture were dried at 363 K, dispersed, and subjected to heat treatment under free air access conditions at 873 (100 h) and 1073 K (50 h). To identify the samples and determine the completeness of interaction between the reagents and the absence of foreign phases in the samples, the phosphates were studied by X-ray diffraction, electron microscopy, and microprobe analysis.

The X-ray diffraction patterns of the $Pb_{0.5}Zr_2(PO_4)_3$ and $PbMg_{0.5}Zr_{1.5}(PO_4)_3$ samples were recorded on a Shimadzu XRD-6000 diffractometer (CuK_α radiation, $\lambda = 1.54178$ Å) within a range of angles $2\theta = 10°–80°$ (scan step, 0.02°) with exposure for 6 s per point. The X-ray diffraction patterns of $Pb_{0.5}Zr_2(PO_4)_3$ for structural studies were taken at 173 and 473 K, and the X-ray diffraction pattern of $PbMg_{0.5}Zr_{1.5}(PO_4)_3$ for the calculation of crystallographic characteristics was recorded at 298.15 K. The processing of X-ray diffraction patterns and the refinement of structures were performed by the Rietveld method [8] using the RIETAN-97 software [9]. The profiles of peaks were approximated by the modified pseudo-Voigt function (Mod-TCH pV). The conditions used for the recording and processing of X-ray diffraction patterns provided the detection of crystalline phases at their content in the sample of no less than 1%

The chemical composition and homogeneity of the synthesized $Pb_{0.5 + x}Mg_xZr_{2 - x}(PO_4)_3$ samples ($x = 0$, 0.5) were monitored on a JEOL JSM-7600F scanning electron microscope (SEM) with a field-emission electron gun (Schottky cathode). The microscope was equipped with a microanalysis system, i.e., a Premium OXFORD X-Max 80 energy dispersive spectrometer with a semiconductor silicon drift detector. The precision of determining the elemental composition of samples was 0.5–2.5 mol %.

The heat capacity of $Pb_{0.5}Zr_2(PO_4)_3$ in the temperature range 8–300 K was measured on a BKT-3.07 fully automated adiabatic vacuum calorimeter (Termis) [10] as described in [11]. Liquid helium and nitrogen were used as cooling agents. An ampoule with the substance was filled with dry helium as a heat transfer gas to a pressure of 40 kPa at room temperature. The calorimeter was tested for performance reliability by measuring the C_p^0 of a copper reference sample of specialty pure grade, synthetic corundum, and benzoic acid of K-3 grade. The measurement instruments and method provided the possibility to estimate the heat capacities of compounds with an error of ±2% at temperatures below 15 K, ±0.5% within a range of 15–40 K, and ±0.2% in the region of 40–300 K and determine the temperatures and enthalpies of phase transitions with an accuracy of ±0.01 K and ±0.2%, respectively. The calorimetric ampoule of the adiabatic calorimeter was filled with 1.47266 g of the studied compound. The heat capacity of the measured sample was 40–50% of the total heat capacity of the calorimetric ampoule with the substance.

The heat capacities of phosphates in the region of 195–660 K were measured on a Netzsch Gerätebau DSC204F1 Phoenix differential scanning calorimeter. The design of the DSC204F1 calorimeter and its operation procedure were described in [12, 13]. The performance reliability tests of this calorimeter were performed by standard calibration experiments measuring the thermodynamic melting characteristics of *n*-heptane, mercury, indium, tin, lead, bismuth, and zinc. The measurement instruments and method provided the possibility to estimate the temperatures and enthalpies of phase transitions with an error of ±0.5 K and ±1%, respectively. The heat capacity of the studied phosphates was determined by the ratio method [13]. Corundum was used as a standard reference. The ampoule with the substance was heated at an average rate of 5 K/min in an argon atmosphere. The C_p^0 esti-

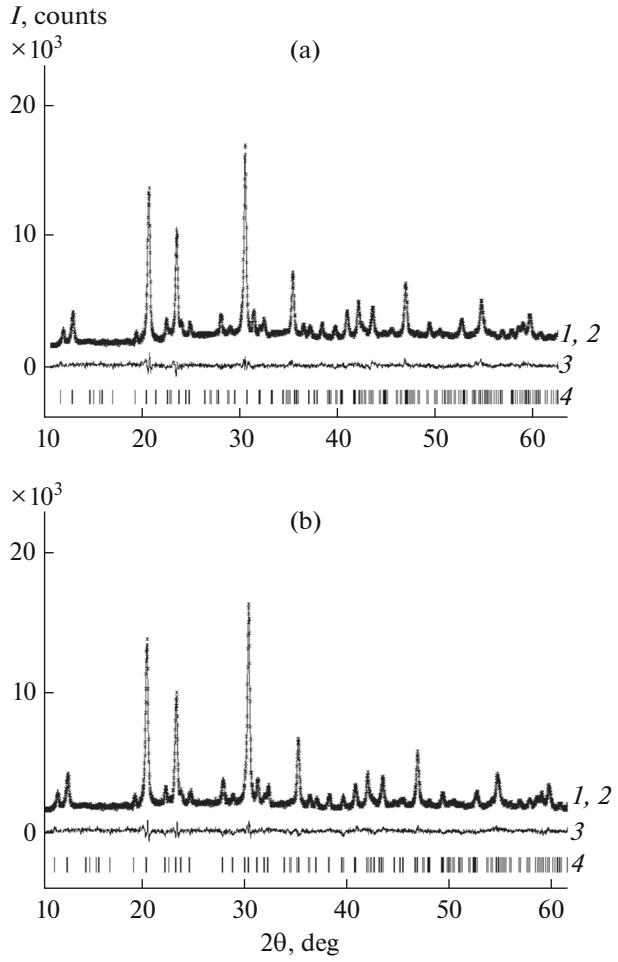

Fig. 1. Experimental (*1*), calculated (*2*), difference (*3*), and stroke (*4*) X-ray diffraction patterns of phosphate $Pb_{0.5}Zr_2(PO_4)_3$ at temperatures of (a) 173 and (b) 473 K.

mation error by the described method was less than ±2%.

RESULTS AND DISCUSSION

Characterization of the Samples

The synthesized $Pb_{0.5+x}Mg_xZr_{2-x}(PO_4)_3$ (x = 0, 0.5) samples represent colorless polycrystalline powders. According to powder X-ray diffraction data, the synthesized phosphates are single phases, crystallize in the NZP structural type, and are identical to the phases described in [6]. Their X-ray diffraction patterns were indexed within space group $R\bar{3}$ (Fig. 1, Tables 1 and 2). The content of impurities in the studied samples does not exceed the detection limit under the given conditions used for the recording and Rietveld refinement of X-ray diffraction patterns (1%). The homogeneity of the $Pb_{0.5+x}Mg_xZr_{2-x}(PO_4)_3$ phosphate samples (x = 0, 0.5) was confirmed by the electron microscopy data (Fig. 2). Their chemical

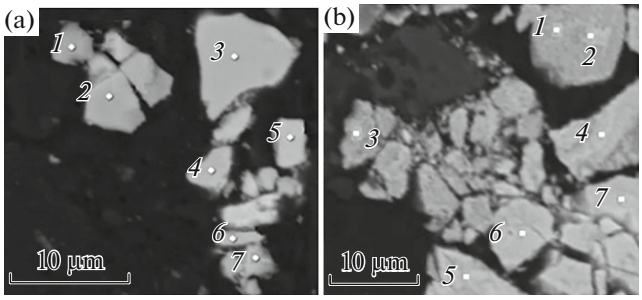

Fig. 2. Electron microscopy results for (a) $Pb_{0.5}Zr_2P_3O_{12}$ and (b) $PbMg_{0.5}Zr_{1.5}P_3O_{12}$.

composition, according to microprobe analysis data, corresponds to the theoretical values within method error (Tables 3 and 4).

Heat Capacity–Temperature Dependence and Polymorphic Transitions

The heat capacity of $Pb_{0.5}Zr_2(PO_4)_3$ was studied by adiabatic vacuum calorimetry (8–300 K, 110 experimental values of C_p^0) and differential scanning (195–660 K) calorimetry (Fig. 3). Experimental values of C_p^0 were smoothed with the use of power and semi-logarithmic polynomials such that the mean-square deviation of experimental points from the smoothed $C_p^0 = f(T)$ curves was less than the error of heat capacity measurements. For example, the heat capacity of $Pb_{0.5}Zr_2(PO_4)_3$ can be described by the following equations (C_p^0 J/(mol K)):

$$\ln C_p^0 = 5.518527 + 24.74717\ln(T/30) + 92.14430[\ln(T/30)]^2 + 184.9730[\ln(T/30)]^3 + 196.7086[\ln(T/30)]^4 + 106.4614[\ln(T/30)]^5 + 230.3970[\ln(T/30)]^6$$

in the temperature range 8–20 K,

$$C_p^0 = 26.42048 + 45.29058\ln(T/30) + 31.49051[\ln(T/30)]^2 - 4.823553[\ln(T/30)]^3 - 2.324907[\ln(T/30)]^4 + 1.513020[\ln(T/30)]^5 + 3.097185[\ln(T/30)]^6$$

in the range 20–50 K,

$$C_p^0 = 375.9106 - 3267.399\ln(T/30) + 12817.11[\ln(T/30)]^2 - 25702.30[\ln(T/30)]^3 + 28313.25[\ln(T/30)]^4 - 16203.82[\ln(T/30)]^5 + 3773.261[\ln(T/30)]^6$$

at 50–80 K,

Table 1. Recording conditions and refinement results for the crystal structure of $Pb_{0.5}Zr_2(PO_4)_3$

T, K	173	473
Space group	$R\bar{3}$ (No. 148)	
Z	6	
Range of 2θ angles, deg	10–80	
Unit cell parameters		
a, Å	8.7009(4)	8.6996(16)
c, Å	23.4822(11)	23.479(3)
V, Å^3	1539.57(13)	1538.9(4)
Number of reflections	295	301
Number of refined parameters*	23 + 28	23 + 28
Reliability factors, %:		
R_{wp}; R_p	3.47; 2.75	3.48; 2.75
S	1.41	1.39

* The first number is the background and profile parameters, scale factor, and unit cell parameters; and the second number is the position and thermal parameters of atoms and their populations.

Table 2. Crystallographic characteristics of $PbMg_{0.5}Zr_{1.5}(PO_4)_3$ at 298.15 K

a, Å	c, Å	V, Å^3
8.6997(4)	23.4591(8)	1537.63(15)

Table 3. Microprobe analysis results for $Pb_{0.5}Zr_2P_3O_{12}$

Point no.	O	P	Zr	Pb
1	12	3.02	2.06	0.52
2	12	2.94	2.05	0.48
3	12	2.97	1.95	0.54
4	12	2.96	2.06	0.53
5	12	2.99	2.08	0.5
6	12	3.04	2.03	0.54
7	12	3.03	1.98	0.52
Average composition	12	3.03(4)	2.03(4)	0.52(2)

Table 4. Microprobe analysis results for $PbMg_{0.5}Zr_{1.5}P_3O_{12}$

Point no.	O	P	Mg	Zr	Pb
1	12	3.06	0.48	1.54	0.97
2	12	2.95	0.49	1.53	1.03
3	12	3.03	0.47	1.49	1.03
4	12	2.98	0.53	1.53	0.97
5	12	3.05	0.5	1.48	1.01
6	12	3.04	0.47	1.54	0.97
7	12	2.99	0.51	1.51	0.98
Average composition	12	3.02(4)	0.49(2)	1.52(2)	0.99(3)

$$C_p^0 = -890.1582 + 1588.630(T/30) - 1102.190(T/30)^2 + 409.6157(T/30)^3 - 83.89098(T/30)^4 + 8.984215(T/30)^5 - 0.3939832(T/30)^6$$

in the range 80–150 K, and

$$C_p^0 = -9971.374 + 9698.560(T/30) - 3877.457(T/30)^2 + 825.8579(T/30)^3 - 98.45857(T/30)^4 + 6.225879(T/30)^5 - 0.1631033(T/30)^6$$

at 150–300 K.

All C_p^0 experimental points and the smoothed curve for $Pb_{0.5}Zr_2(PO_4)_3$ are shown in Fig. 3. According to DSC data, the studied phosphate experiences a reversible phase transition in the range 256–426 K. In compliance with the McKallaf thermodynamic classification of phase transitions, it may be classified with G-type transitions. This transition does not appear up to 300 K when the heat capacity of the same $Pb_{0.5}Zr_2(PO_4)_3$ sample is measured in the adiabatic calorimeter, probably, due to its nonequilibrium character (it does not appear under near-equilibrium recording conditions).

To clarify the nature of the considered phase transition, the structural study of $Pb_{0.5}Zr_2(PO_4)_3$ was performed at 173 and 473 K by the Rietveld method using the powder X-ray diffraction data (Fig. 1, Table 2). The initial data used for structural refinement at the mentioned temperatures were the coordinates of atoms in the structure of phosphate $Cu_{0.5}Mn_{0.25}Zr_2(PO_4)_3$ (NZP, space group $R\bar{3}$ [14]). The coordinates of atoms in the refined models are given in Table 5.

Table 5. Coordinates of atoms in the structure of $Pb_{0.5}Zr_2(PO_4)_3$

Atom/position	x		y		z	
	173 K	473 K	173 K	473 K	173 K	473 K
Pb*/18f	0.02(6)	−0.033 (26)	0.00(12)	−0.034 (22)	0.0044(11)	0.0035(13)
Zr(1)/6*c*	0	0	0	0	0.15061(18)	0.15073(20)
Zr(2)/6*c*	0	0	0	0	0.64726(17)	0.64701(19)
P/18*e*	0.2939(13)	0.2996(13)	0.0201(16)	1.0237(15)	0.2524(6)	0.2455(6)
O(1)/18*f*	0.1701(21)	0.1655(23)	0.9654(22)	0.9585(26)	0.1901(11)	0.1927(10)
O(2)/18*f*	0.073(3)	0.1513(25)	0.859(3)	0.9306(23)	0.7036(7)	0.7024(8)
O(3)/18*f*	0.193(3)	0.2022(25)	0.178(2)	0.1516(22)	0.0840(9)	0.0980(8)
O(4)/18*f*	0.8293(28)	0.7999(26)	0.7724(23)	0.7733(27)	0.6114(8)	0.5936(8)

*The occupancy of this position is 0.167.

Both $Pb_{0.5}Zr_2(PO_4)_3$ polymorphs belong to the NZP structural type, and structural refinement was performed in both cases within space group $R\bar{3}$ characterized by the splitting of M1 crystallographic positions (6*a*) in the cavities inside the polyhedra columns into two types of non-equivalent positions (3*a* and 3*b*).

In the structures of most NZP compounds $M_{0.5}Zr_2(PO_4)_3$ [7], the positions of one type (3*a* or 3*b*) are occupied by M^{2+} cations, and the other type remains vacant. In this case, M^{2+} cations are in an octahedral environment with six metal–oxygen bonds of identical length. However, in the case of $Pb_{0.5}Zr_2(PO_4)_3$, the Pb^{2+} cations occupying the structure cavities have a stereoactive $6s^2$ electron pair, which usually results in the distortion of lead–oxygen polyhedra [15, 16]. The degree of their distortion in the known lead-containing compounds depends on the temperature and their structural features. As a consequence, the Pb^{2+} ions are shifted from the centers of octahedrally coordination cavities (disordered), and the symmetry of their positions decreases to 18*f*.

A fragment of the crystal structure of $Pb_{0.5}Zr_2(PO_4)_3$ at 173 K is shown in Fig. 4a. The NZP framework of this compound is built of ZrO_6 octahedra and PO_4 tetrahedra. Fragments of two octahedra and three tetrahedra form the columns along crystallographic axis *c*. A half of the cavities inside these columns are occupied by Pb^{2+} ions shifted from their center due to slight disordering. The interatomic distances (Table 6) in the coordination polyhedra composing the crystal structure of the studied compound at both temperatures agree with the literature data for the other phosphates with an NZP structure [6, 14].

The results of structure refinement for $Pb_{0.5}Zr_2(PO_4)_3$ at 173 and 473 K showed that, as the temperature grows, the degree of ordering for the lead cations sustains an increase accompanied by stronger distortion in the PbO_6 octahedra (Fig. 4b, Table 6). Hence, the polymorphic transitions on the heat capacity curves of the studied phosphates occur due to

Table 6. Selected interatomic distances in the polyhedra forming the structure of $Pb_{0.5}Zr_2(PO_4)_3$

T = 173 K		T = 473 K	
bond	d, Å	bond	d, Å
Pb–O(3)	2.41(3)	Pb–O(3)	2.62(2)
Pb–O(3')	2.43 (6)	Pb–O(3')	2.70(5)
Pb–O(3'')	2.53(4)	Pb–O(3'')	2.72(8)
Pb–O(3''')	2.59 (5)	Pb–O(3''')	2.90(7)
Pb–O(3'''')	2.68(6)	Pb–O(3'''')	2.92(5)
Pb–O(3''''')	2.70(3)	Pb–O(3''''')	2.99(6)
Zr(1)–O(1) (×3)	1.894(21)	Zr(1)–O(1) (×3)	1.922(23)
Zr(1)–O(3) (×3)	2.250 (19)	Zr(1)–O(3) (×3)	2.012(17)
Zr(1)–O(4) (×3)	1.974 (23)	Zr(1)–O(4) (×3)	2.141(19)
Zr(1)–O(2) (×3)	2.107 (27)	Zr(1)–O(2) (×3)	2.252(19)
P–O(3)	1.413(21)	P–O(3)	1.426(17)
P–O(2)	1.443(29)	P–O(2)	1.436(12)
P–O(4)	1.535 (26)	P–O(4)	1.599(25)
P–O(1)	1.636(27)	P–O(1)	1.699(27)

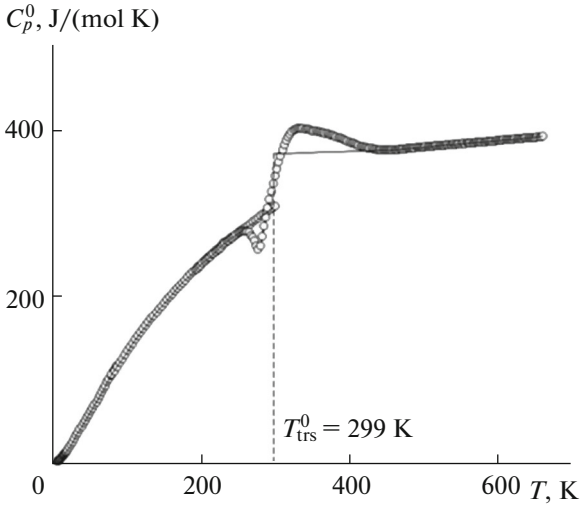

Fig. 3. Heat capacity of $Pb_{0.5}Zr_2(PO_4)_3$ versus temperature.

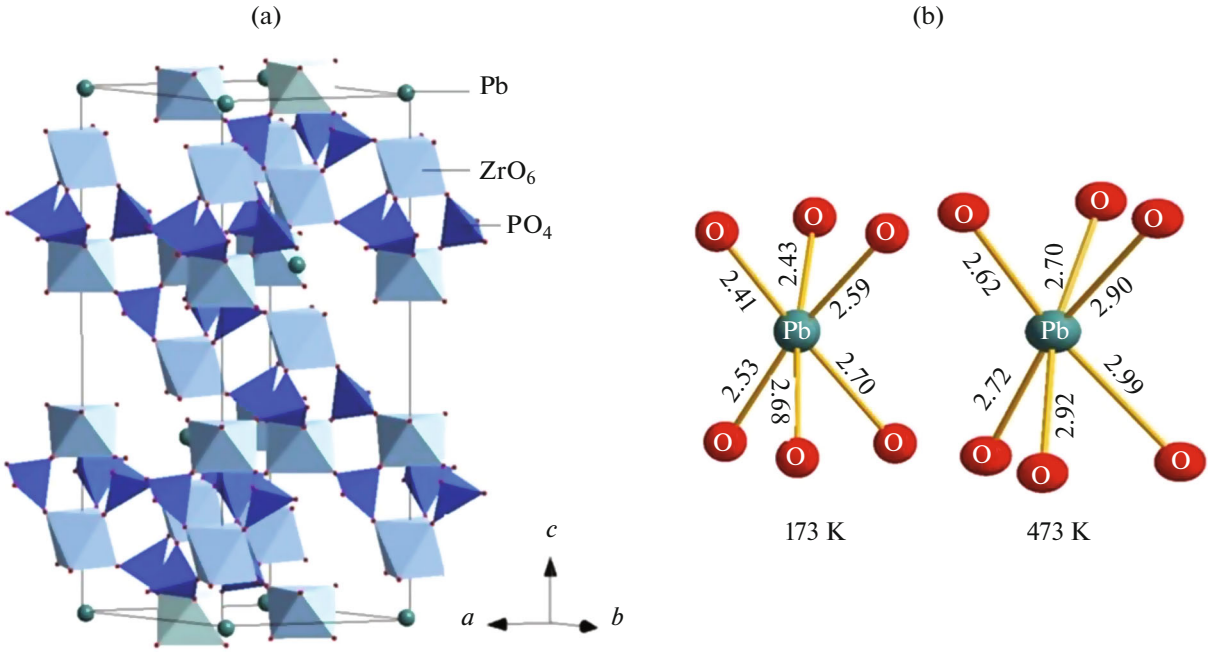

Fig. 4. Structure of $Pb_{0.5}Zr_2(PO_4)_3$: (a) crystal structure fragment at 173 K and (b) distortion of PbO_6 octahedra at 173 and 473 K.

an increase in the disordering of lead cation positions in the NZP structure cavities.

The heat capacity–temperature dependence for $PbMg_{0.5}Zr_{1.5}(PO_4)_3$ in the range 195–660 K (Fig. 5) is similar to the above-considered dependence for $Pb_{0.5}Zr_2(PO_4)_3$. This compound also experiences a polymorphic phase transition, but at lower temperatures (255–315 K), and a heat capacity jump is less pronounced in this region. This thermal behavior of $PbMg_{0.5}Zr_{1.5}(PO_4)_3$ can be explained by the fact that the Pb^{2+} cations in its structure completely populate the M1 cavities inside the columns of framework-forming polyhedra and, therefore, the possibilities of structural distortions due to the displacement of these ions are more limited.

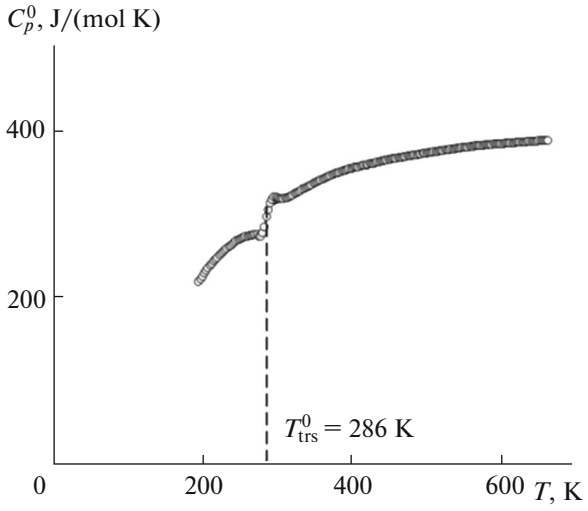

Fig. 5. Heat capacity of $PbMg_{0.5}Zr_{1.5}(PO_4)_3$ versus temperature.

Heat Capacity and Thermodynamic Functions

Except the regions of transitions, the heat capacity of phosphates has no singularities and smoothly rises throughout the range of temperatures studied. To calculate the thermodynamic functions of $Pb_{0.5}Zr_2(PO_4)_3$, the temperature dependence of its heat capacity was extrapolated to 0 K by the Debay function $C_p^0 = nD(\theta_D/T)$, where D is the Debay function symbol and $n = 3$, $\theta_D = 88.4$ K are fitted parameters. Together with the mentioned parameters, this equation describes the experimental values of C_p^0 in the range 8–12 K with an error of 2.4%. It was assumed that Eq. (2) reproduced the values of C_p^0 at $T < 8$ K with the same error.

The low-temperature heat capacity data (30–50 K) were processed with consideration for the multifractality of the vibrational states of atoms [17, 18]. The fractal dimension D [19, 20] in the multifractal model serves as an indirect characteristic of the structural topology of solids and provides the possibility to judge the geometric character of their structure: $D = 1$ for solids with a chain structure, $D = 2$ for a layered structure, and $D = 3$ for a spatial structure. Assuming without appreciable accuracy loss that $C_p^0 = C_v^0$ at $T < 50$ K and using the experimental heat capacity data, we find with an error of 1.0% that the studied phosphate

Table 7. Standard thermodynamic functions of crystalline $Pb_{0.5}Zr_2(PO_4)_3$ (FW = 570.957 g/mol, p^0= 0.1 MPa)

T, K	C_p^0, J/(mol K)	$\left[H^0(T) - H^0(0)\right]$, kJ/mol	$S^0(T)$, J/(mol K)	$-\left[G^0(T) - H^0(0)\right]$, kJ/mol
		Crystal **I**		
0	0	0	0	0
5	0.352	0.000400	0.117	0.000146
10	2.60	0.00680	0.910	0.00232
20	12.87	0.08060	5.611	0.03165
30	26.42	0.2743	13.28	0.1239
40	41.83	0.6154	22.99	0.3041
60	71.15	1.747	45.53	0.9847
80	103.5	3.492	70.41	2.140
100	129.5	5.822	96.29	3.807
120	154.7	8.668	122.2	5.992
140	177.4	11.99	147.7	8.692
160	198.2	15.75	172.8	11.90
180	217.2	19.91	197.3	15.60
200	234.7	24.43	221.1	19.78
220	250.8	29.29	244.2	24.44
240	265.9	34.46	266.7	29.55
260	278.3	39.89	288.4	35.10
280	291.4	45.59	309.5	41.08
298.15	303.4	50.99	328.2	46.87
299	303.9	51.24	329.1	47.15
		Crystal **II**		
299	367.7	51.24	329.1	47.15
300	368	51.6	330	47.5
320	368	59.0	354	54.3
340	369	66.3	376	61.6
360	369	73.7	397	69.4
380	370	81.1	417	77.5
400	370	88.5	436	86.1
420	371	95.9	455	95.0
440	372	103	472	104
460	372	111	488	114
480	374	118	504	124
500	375	126	520	134
520	377	133	534	145
540	379	141	549	155
560	380	148	562	166
580	382	156	576	178
600	383	164	589	190
620	385	171	601	201
640	386	179	613	214
660	388	187	625	226

Table 8. Heat capacities smoothed with polynomials for crystalline $PbMg_{0.5}Zr_{1.5}(PO_4)_3$ (FW = 641.098 g/mol, p^0 = 0.1 MPa)

T, K	C_p^0, J/(mol K)	T, K	C_p^0, J/(mol K)
Crystal **I**		380	347
195	214	400	353
200	222	420	357
220	245	440	361
240	261	460	365
260	272	480	369
280	280	500	371
286	282	520	374
Crystal **II**		540	377
286	307	560	379
298.15	312	580	381
300	312	600	383
320	321	620	384
340	330	640	385
360	340	660	386

$Pb_{0.5}Zr_2(PO_4)_3$ has $D = 3$, which corresponds to a spatial (framework) structure of this compound.

The enthalpies $[H^0(T) - H^0(0)]$ and entropies $S^0(T)$ of $Pb_{0.5}Zr_2(PO_4)_3$ were calculated via the numerical integration of the corresponding $C_p^0 = f(T)$ and $C_p^0 = f(\ln T)$ dependences, and the Gibbs functions $[G^0(T) - H^0(0)]$ were estimated from the enthalpies and entropies of compounds at the corresponding temperatures. The smoothed heat capacities and thermodynamic functions of $Pb_{0.5}Zr_2(PO_4)_3$ are given in Table 7. The $PbMg_{0.5}Zr_{1.5}(PO_4)_3$ heat capacities smoothed with polynomials are listed in Table 8.

The heat capacity of the studied phosphates at high temperatures approaches the values estimated by the Dulong–Petit law $C_p^0 = 3RN$, where R is the universal gas constant and N is the number of atoms in a formula unit. The calculated and experimental (at 660 K) heat capacities were 436.5 and 387.8 J/(mol K) for $Pb_{0.5}Zr_2(PO_4)_3$ and 449.0 and 416 J/(mol K) for $PbMg_{0.5}Zr_{1.5}(PO_4)_3$.

Using the absolute entropies of crystalline phosphate $S^0(Pb_{0.5}Zr_2(PO_4)_3$, cr, 298.15 K) = 328.2 ± 1.0 J/(mol K) (Table 7) and corresponding simple compounds [21, 22] S^0(Pb, cr, 298.15 K) = 64.80 ± 0.30 J/(mol K), S^0(Zr, cr, 298.15 K) = 38.994 ± 0.167 J/(mol K), S^0(P, cr, 298.15 K) = 41.09 ± 0.25 J/(mol K), and $S^0(O_2$, gas, 298.15 K) = 205.152 ± 0.005 J/(mol K), we calculated the standard formation entropy of the studied compound $\Delta_f S^0(Pb_{0.5}Zr_2(PO_4)_3$, cr, 298.15 K) = −1136.4 ± 1.3 J/(mol K). The found value corresponds to the process

$$0.5Pb(cr) + 2Zr(cr) + 3P(cr, white) + 6O_2(gas) = Pb_{0.5}Zr_2(PO_4)_3 (cr).$$

CONCLUSIONS

Crystalline phosphates $Pb_{0.5}Zr_2(PO_4)_3$ and $PbMg_{0.5}Zr_{1.5}(PO_4)_3$ of NZP structural type were synthesized by the sol–gel method. The isobaric heat capacities of $Pb_{0.5}Zr_2(PO_4)_3$ in the temperature region of 8–660 K and $PbMg_{0.5}Zr_{1.5}(PO_4)_3$ in the range 195–660 K were studied for the first time. Phase transitions of G type were observed in the heat capacity–temperature dependences of both phosphates. Based on the results of the structural study of $Pb_{0.5}Zr_2(PO_4)_3$ at 173 and 473 K, these polymorphic transitions were elucidated to occur due to an increase in the position disordering of lead cations in NZP structure cavities. The thermodynamic functions of $Pb_{0.5}Zr_2(PO_4)_3$ were calculated in the region from $T \to 0$ to 660 K, and the standard enthalpy of its formation from simple compounds at 298.15 K was determined. Based on the low-temperature heat capacity, the fractal dimension of $Pb_{0.5}Zr_2(PO_4)_3$ was calculated, and the conclusion about the applicability of this model to framework NZP compounds was made.

FUNDING

This work was supported by the Russian Foundation for Basic Research (project nos. 19-33-90075 and 18-29-12063) and by the Ministry of Science and Higher Education of the Russian Federation (state assignment no. 4.8337.2017/BCh).

CONFLICT OF INTERESTS

The authors declare that they have no conflict of interests.

REFERENCES

1. M. I. Kimpa, M. Z. H. Mayzan, J. A. Yabagi, et al., IOP Conf. Ser.: Earth Env. Sci. 140, 012156 (2018). https://doi.org/10.1088/1755-1315/140/1/012156
2. L. Small, J. Wheeler, J. Ihlefeld, et al., J. Mater. Chem. A **6**, 9691 (2018). https://doi.org/10.1039/C7TA09924J
3. V. I. Pet'kov, Russ. Chem. Rev. **81**, 606 (2012). https://doi.org/10.1070/RC2012v081n07ABEH004243
4. B. E. Scheetz, D. K. Agrawal, E. Breval, and R. Roy, Waste Manag. **14**, 489 (1994).
5. V. Pet'kov, E. Asabina, V. Loshkarev, and M. Sukhanov, J. Nucl. Mater. **471**, 122 (2016). https://doi.org/10.1016/j.jnucmat.2016.01.016
6. E. Asabina, V. Pet'kov, P. Mayorov, et al., Pure Appl. Chem. **89**, 523 (2017). https://doi.org/10.1515/pac-2016-1005

7. V. I. Pet'kov, V. S. Kurazhkovskaya, A. I. Orlova, and M. L. Spiridonova, Crystallogr. Rep. **47**, 736 (2002). https://doi.org/10.1134/1.1509386
8. H. M. Rietveld, Acta Crystallogr. **22**, 151 (1967).
9. Y. I. Kim and F. Izumi, J. Ceram. Soc. Jpn. **102**, 401 (1994).
10. V. M. Malyshev, G. A. Mil'ner, E. L. Sorokin, et al., Pribory Tekh. Eksp. **6**, 195 (1985).
11. R. M. Varushchenko, A. I. Druzhinina, and E. L. Sorkin, J. Chem. Thermodyn. **29**, 623 (1997).
12. G. W. H. Hohne, W. F. Hemminger, and H. F. Flammersheim, Differential Scanning Calorimetry (Springer, Berlin/Heidelberg, 2003).
13. V. A. Drebushchak, J. Therm. Anal. Calorim. **79**, 213 (2005).
14. A. Mouline, M. Alami, R. Brochu, et al., J. Solid State Chem. **152**, 453 (2000). https://doi.org/10.1006/jssc.2000.8711
15. S. A. Larregola, J. A. Alonso, J. C. Pedregosa, et al., Dalton Trans., No. 28, 5453 (2009). https://doi.org/10.1039/B821688F
16. S. A. Larregola, J. A. Alonso, M. Alguero, et al., Dalton Trans. **39**, 5159 (2010). https://doi.org/10.1039/C0DT00079E
17. T. S. Yakubov, Dokl. Akad. Nauk SSSR **310**, 145 (1990).
18. A. D. Izotov, O. V. Shebershneva, and K. S. Gavrichev, Proceedings of the All-Russia Conference on Thermal Analysis and Calorimetry, Kazan, 1996 (Kazan, 1996), p. 200.
19. V. V. Tarasov, Zh. Fiz. Khim. **24**, 111 (1950).
20. V. V. Tarasov and G. A. Yunitskii, Zh. Fiz. Khim. **39**, 2077 (1965).
21. CODATA Key Values for Thermodynamics, Ed. by J. D. Cox, D. D. Wagman, and V. A. Medvedev (New York, 1984).
22. Thermal Constants of Materials, Ed. by V. P. Glushko (Nauka, Moscow, 1965–1981) [in Russian].

Translated by E. Glushachenkova